Journal of Molecular Graphics and Modelling 29 (2010) 21–31

Contents lists available at ScienceDirect

Journal of Molecular Graphics and Modelling

journal homepage: www.elsevier.com/locate/JMGM

Insights into designing the dual-targeted HER2/HSP90 inhibitors

Chien-Yu Chen [a], Calvin Yu-Chian Chen [a,b,c,*]

[a] Laboratory of Computational and Systems Biology, School of Chinese Medicine, China Medical University, Taichung 40402, Taiwan, ROC
[b] Department of Bioinformatics, Asia University, Taichung 41354, Taiwan, ROC
[c] Computational and Systems Biology, Massachusetts Institute of Technology, Cambridge, MA 02139, USA

ARTICLE INFO

Article history:
Received 2 December 2009
Received in revised form 7 April 2010
Accepted 9 April 2010
Available online 18 April 2010

Keywords:
Dual-targeted inhibitors
HER2
HSP90
QSAR
Pharmacophore

ABSTRACT

Heat shock protein 90 (HSP90) and human epidermal growth factor receptor 2 (HER2) are two key cancer markers actively involved in several signal pathways for cancer cell growth. In this study, we focused on the designing of dual-targeted HSP and HER2 inhibitors. Comparative molecular field analysis (CoMFA), comparative molecular similarity indices analysis (CoMSIA), and pharmacophore analysis were employed for generating the activity prediction models. The results of CoMFA model showed highly predictive r^2 value with 0.922 and 0.885 in HSP90 and HER2, respectively. In CoMSIA model, the r^2 values were 0.967 and 0.936 in HSP90 and HER2, respectively. The contour maps of both targets showed that there were similar regions of bulky favored area. Additionally, the Hypogen results for HER2 showed high cost difference as 59.13 and *r*-value as 0.909. At the C2 position of the benzene ring, the HER2 model favored steric bulkier substitutes more than HSP90. The Hypogen results for HSP90 also showed reliable values in cost difference, 85.82 and *r*-value, 0.902. Overall, we investigated the significances of QSAR models and pharmacophore features for designing the HER2/HSP90 dual-targeted inhibitors.

1. Introduction

Heat shock protein 90 (HSP90) is a housekeeping molecular chaperone required by many oncogenic signaling proteins to ensure their stabilities and functions [1]. Its roles involve supporting functional maturation of signaling proteins, transporting proteins between cellular compartments, suppressing protein aggregation, and most importantly facilitating protein re-folding and turnover [2–4]. Notable HSP90-dependent transcription factors and kinases include receptor tyrosine kinases (RTKs), hypoxia-inducible factor-1 (HIF-1), Src kinases, Raf-1, Akt proteins, and cyclin dependent kinase (CDK) 4 [5].

It was suggested that HSP90 inhibitors could block the cellular processes involved in cancer invasion and metastasis [1,6,7]. Recently, fragments of HSP90 have been identified at the cell surface and have been determined to participate in cancer invasion and metastasis [1]. The amount of HSP90 on cell surface correlates with environmental stress. This event could be explained as a cell survival mechanism [8].

To transform a healthy cell to exhibit cancer characteristics requires multiple signal transductions [9,10]. EGFR, RTKs, and C-Met were reported as key regulators of normal cellular functions [11–15]. EGFR and HER2 are cell surface receptor tyrosine kinases (TKs). Both transport growth signals by dimerization with HER family receptors. The heterodimerization of HER2 induces a more potent activation than EGFR homodimerization. When EGFR and HER2 over-express in tumor cells, aggressive tumor cell growth, including proliferation and invasion, will be observed.

In last few years, researches on virtual drug design and protein configuration determination are gaining attention [16–20]. Drug development, now, not only focuses on selectively, but also on targets specificity [21–24]. Multi-targeted therapeutic compounds have the advantages of effectively inhibiting or activating multiple pathways, and can also avoid possible drug-drug interaction that might associate between single-targeted drugs. In cancer chemotherapy, drugs with multi-targets can inhibit cancer growth by blocking different signal pathways [25–27]; one notable example is the anticancer drug, ZD6474, that targets both EGFR-1 and VEGFR-2 tyrosine kinase [28]. However, this concept is new and has many problems to overcome [29]. Overall, the aim of this study is to construct predictive models that could be used to design inhibitors targeting HSP90 and HER2.

2. Methodology

2.1. Data set

In this study, 48 compounds from Llauger's studies [30,31] that have inhibitory activities toward HSP90 and HER2 were used as the

* Corresponding author at: Computational and Systems Biology, Massachusetts Institute of Technology, Cambridge, MA 02139, USA. Tel.: +1 617 353 7123.
E-mail addresses: ycc@mail.cmu.edu.tw, ycc929@MIT.EDU (C.Y.-C. Chen).

1093-3263/$ – see front matter © 2010 Elsevier Inc. All rights reserved.
doi:10.1016/j.jmgm.2010.04.002

Table 1
The molecular structures of training set.

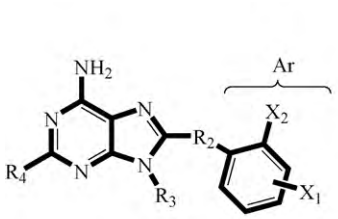

10n-29

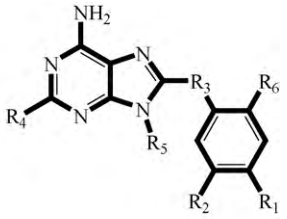

B9-B33

Name	Ar	R2	R3	R4
11l	2,4-Cl2-Ph	S		H
11m	2,5-Me2-Ph	S		H
11o	2,5-OMe2-Ph	S		H
11p	2-Br-5-OMe-Ph	S		H
11q	2-I-5-OMe-Ph	S		H
11s	3,5-Cl2-Ph	S		H
11u	2,4,5-Cl3-Ph	S		H
11v	2-Br-4,5-(OCH2O)-Ph	S		H
11w1	3,4,5-OMe3-Ph	S		H
11w2	3,4,5-OMe3-Ph	S	Butyl	H
11w3	3,4,5-OMe3-Ph	S	2-Isopropoxy-ethyl	H
12a	2-Cl-5-OMe-Ph	S		H
12b	2-Cl-3,4,5-OMe3-Ph	S		H
12c	2,4-Cl2-5-OMe-Ph	S	2-Isopropoxy-ethyl	H
12e	2,6-Cl2-3,4,5-OMe3-Ph	S	2-Isopropoxy-ethyl	H
13	2-I-3,4,5-OMe3-Ph	S		H
20a	3,4,5-OMe3-Ph	S	Pent-4-ynyl	F

Name	R1, R2	R3	R4	R5	R6
B9	–OCH_2O–	S	H		I
B10	–OCH_2O–	S	H		Br
B11	–OCH_2O–	S	H		I
B12	–OCH_2O–	S	H		Br
B21	–OCH_2O–	CH2	F		I
B22	–OCH_2O–	CH2	F		Br
B23	–OCH_2O–	CH2	F		Cl
B25	–OCH_2O–	CH2	F		I
B31	OMe, OMe	CH2	F		I
B32	OMe, OMe	CH2	F		Br
B33	OMe, OMe	CH2	F		Cl

Table 2
The molecular structures of test set.

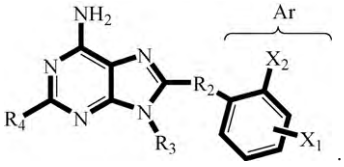

Name	Ar	R2	R3	R4
4	2-Cl-3,4,5-OMe_3-Ph	CH_2	Pent-4-ynyl	F
11a	2-OMe-Ph	S		H
11i	4-Pyrrolyl-Ph	S		H
28a	3-OMe-Ph	SO_2	Pent-4-ynyl	H
28b	3-OMe-Ph	SO_2	2-Isopropoxy-ethyl	H
28c	3-OMe-Ph	SO_2	Butyl	H
28d	3,4,5-OMe_3-Ph	SO_2	Butyl	H
28e	3,4,5-OMe_3-Ph	SO_2	Pent-4-ynyl	H
28f	3,4,5-OMe_3-Ph	SO_2	2-Isopropoxy-ethyl	H
30	3,4,5-OMe_3-Ph	CH_2	Pent-4-ynyl	H
31	3,4,5-OMe_3-Ph	CH_2	2-Isopropoxy-ethyl	H
32	3,4,5-OMe_3-Ph	CH_2	Pent-4-ynyl	F

model training set (Table 1), and an additional set of 12 compounds were selected as test set (Table 2). The inhibitory activity of these compounds for HER2 was obtained indirectly from Llauger's studies, but we believed the structural–activity relationship can still be deduced from these activity data. These compounds were drawn by ChemDraw Ultra 10.0 (Cambridgesoft Inc., USA) and transformed to 3D molecule models by Chem3D Ultra 10.0 (Cambridgesoft Inc., USA).

2.2. 3D-QSAR modeling by CoMFA and CoMSIA

Comparative molecular field analysis (CoMFA) and comparative molecular similarity indices analysis (CoMSIA) were performed in Sybyl 8.0 (Tripos Inc., St. Louis, MO, USA). Lennard-Jones potential and Coulombic potential were employed to calculate steric and electrostatic interaction energies. In CoMFA, the biological activities of the compounds were correlated with their steric and electrostatic energies. Additionally, hydrophobic force field, hydrogen bond acceptor force field, and hydrogen bond donor force field from CoMSIA were also considered in this study. The two 3D-QSAR models were further analyzed in leave-one-out (LOO) and evaluated by cross-validated correlation coefficient (q^2) and non-cross-validated correlation coefficient (r^2). The correlation between the force field and biological activities was calculated by partial least squares (PLSs) method.

2.3. Pharmacophore hypotheses generation (Hypogen)

The protocol, pharmacophore hypotheses generation (Hypogen), was performed by Discovery studio 2.1 (Accelrys, San Diego, USA). All parameters were set to default. The most active compound and the least active compound in the data set were selected to be the fixed hypothesis and the null hypothesis, respectively. Other compounds in the data set were aligned to generate common features and pharmacophore hypotheses. The total costs were used to analyze the results of Hypogen. The fit values were calculated only if the compounds can fit into the hypotheses. Moreover, the fit values could be correlated to the biological activities of the compounds. Additionally, the Fischer's randomization test with 95% confidence level was applied in this study. Root-mean-square deviation was employed to analyze the distances between different pharmacophore features.

2.4. Building homology model and docking study

Based on the information provided on the Swiss-prot databank p04626, the HER2 protein kinase domain is located at sequence 720–987, but the three-dimensional structure of this kinase domain had not been resolved. Thus, we employed epidermal growth factor receptor (EGFR) that shared high identity with HER2 as the modeling template for the protein kinase domain. EGFRs (PDB code: 2GS7, 2J5E, and 2J6M) of the same family were used as template, and their structures were obtained from the protein data bank (PDB). Multiple sequence alignment program, CLUSTAL W, was used in the alignment step. Additionally, the alignment score was calculated by BLOSM.

The parameters for docking experiments are listed in Table S1. The LigandFit program was used to perform all the simulation protocols. During the docking processes, ligands were flexible whereas the receptors were fixed. The ligand flexibility was carried out by *in situ* ligand minimization based on the CHARMm force field. To ensure the structural accuracy of the HER2 model, we docked EGFR inhibitor Iressa into HER2 structure and compared the Iressa docking pose and orientation with the EGFR–Iressa complex (PDB ID:2ITY).

3. Results and discussion

3.1. The results of CoMFA and CoMSIA

The 48 compounds obtained from Llauger's studies [30,31] are shown in Table 1. The scaffolds of 48 compounds are all purine-based. The aligned atoms are shown in Fig. 1. Results from cross-validated PLS analysis are summarized in Table 3. In CoMFA model, the values of q^2 and r^2 for HSP90 were 0.693 and 0.922, respectively. In CoMSIA, similar values were obtained, with q^2 and r^2 equals to 0.659 and 0.967. Exact CoMFA and CoMSIA analysis were applied to HER2. The q^2 and r^2 corresponded to 0.653 and 0.885 in CoMFA and 0.646 and 0.936 in

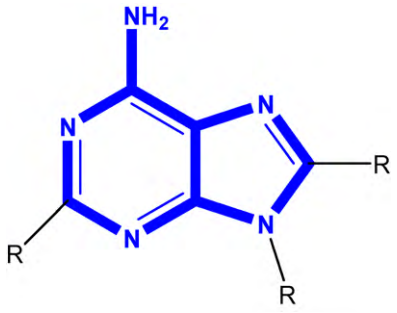

Fig. 1. Scaffold of purine-based compounds. The aligned core atoms are labeled by blue lines. (For interpretation of the references to color in this figure legend, the reader is referred to the web version of the article.)

CoMSIA. Additionally, the test was employed in this analysis. The results of the test set were showed in Tables 4 and 5. The predicted and experimental activities are listed in Tables 6 and 7. These results were used to validate the reliability of our models.

The CoMFA contour maps of HER2 and HSP90 are shown in Fig. 2a and b. The major difference between the two proteins is indicated by the red circle in Fig. 2b. Within the circle, the yellow regions disfavor the addition of bulky substituent at the pent-4-ynyl side chain of anti-HSP90 compounds. In the CoMSIA contour maps, both HER2 and HSP90 (Figs. 2–4) exhibited similar hydrophobic favor regions and hydrophobic disfavor regions. However, in HER2 model (Fig. 2e, Fig. 3e, and Fig. 4e) region, as near by the red region, has smaller hydrogen bond favor regions which could restrict the varieties of substitutes found on this site. Accordingly, a dual-target inhibitor should be designed to meet these two restrictions. In addition, the HER2 CoMSIA model suggests that attaching electronegative substituent near the C2 position of the benzene ring could improve binding affinity. These results are consistent with the biological activities. Specifically, compounds with pent-4-ynyl side chain demonstrate higher activities than other replacements. In fact, the pIC_{50} exp value of compound 11p was 5.84 in HER2 but 7.15 in HSP90. The pIC_{50} exp value of compound 11q was 6.09 in HER2 and 7.3 in HSP90. The pIC_{50} exp value of compound 11v was 6.52 in HER2 and 7.52 in HSP90. The results suggest that the limitation on HER2 is stronger than in HSP90.

3.2. The results of docking study

The result of HER2 modeling can be divided into three parts. Firstly, the sequence alignment showed 65.9% identify and 75.1 similarity between HER2 and EGFR (Fig. S1). Secondly, the plot of verified score (shown in Fig. S2) showed the HER2 model was stable and reliable. Lastly, the Ramachandran plot showed that only

1.865% of residues were outside the region of possible angle formations (Fig. S3). All these results suggested that the HER2 model was reliable.

A comparison between the EGFR–Iressa crystal complex and the HER2–Iressa complex gave a RMSD value of 2.2 (Fig. S4). Based on the RMSD report by Cole et al. [32], a RMSD value between 2 and 3 suggested partial success in modeling. Because we did not re-docked Iressa into EGFR structure, this discrepancy was still reasonable [33]. To further support the results from Hypogen, docking study was performed. The docking poses of compound 11v are shown in Fig. 4e and f. In HER2, compound 11v not only formed a hydrogen bond to Lys34, but also generated π-staking on Phe12 (Fig. 4e). This may lead to π-staking to offer a strong force to stabilize the compound conformation. However, similar interaction of π-staking was not found in HSP90 complex. In contrast, two hydrogen bonds were formed between the HSP90 and compound 11v (as labeled in Fig. 4f). Consistent with the results from Hypogen, the observed bond angle of C–S–C in compound 11v was sharper in HER2 than in HSP90.

Table 3
The PLS index of HSP90 and HER2 by CoMFA and CoMSIA statistics.

Models	HSP90					HER2				
	q^2	Components	r^2	SEE	F	q^2	Components	r^2	SEE	F
CoMFA	0.693	5	0.922	0.333	102.64	0.653	5	0.885	0.331	79.11
CoMSIA	0.659	6	0.967	0.283	120.53	0.646	6	0.936	0.270	101.84

SEE: standard error of estimate; F: F-test value.

Table 4
The CoMFA and CoMSIA test results of HER2.

Name	CoMFA			CoMSIA	
	$pIC_{50\ exp}$	$pIC_{50\ pred}$	Residual	$pIC_{50\ pred}$	Residual
4	5.82	3.489	2.331	2.641	3.1791
11a	3.40	4.786	−1.3865	3.574	−0.1739
11i	3.51	4.831	−1.3207	3.446	0.0641
28a	3.80	4.604	−0.804	4.609	−0.8092
28b	3.77	3.568	0.2017	4.369	−0.5986
28c	3.90	4.476	−0.5757	4.487	−0.5866
28d	3.50	4.18	−0.6795	4.421	−0.9213
28e	3.98	4.174	−0.1944	4.308	−0.3276
28f	3.30	4.113	−0.813	4.261	−0.9615
30	4.83	3.752	1.0782	2.72	2.11
31	4.54	4.085	0.4553	3.015	1.5251
32	4.98	3.786	1.1938	2.776	2.2045

$pIC_{50\ exp}$: experimental pIC_{50}; $pIC_{50\ pred}$: predicted pIC_{50}.

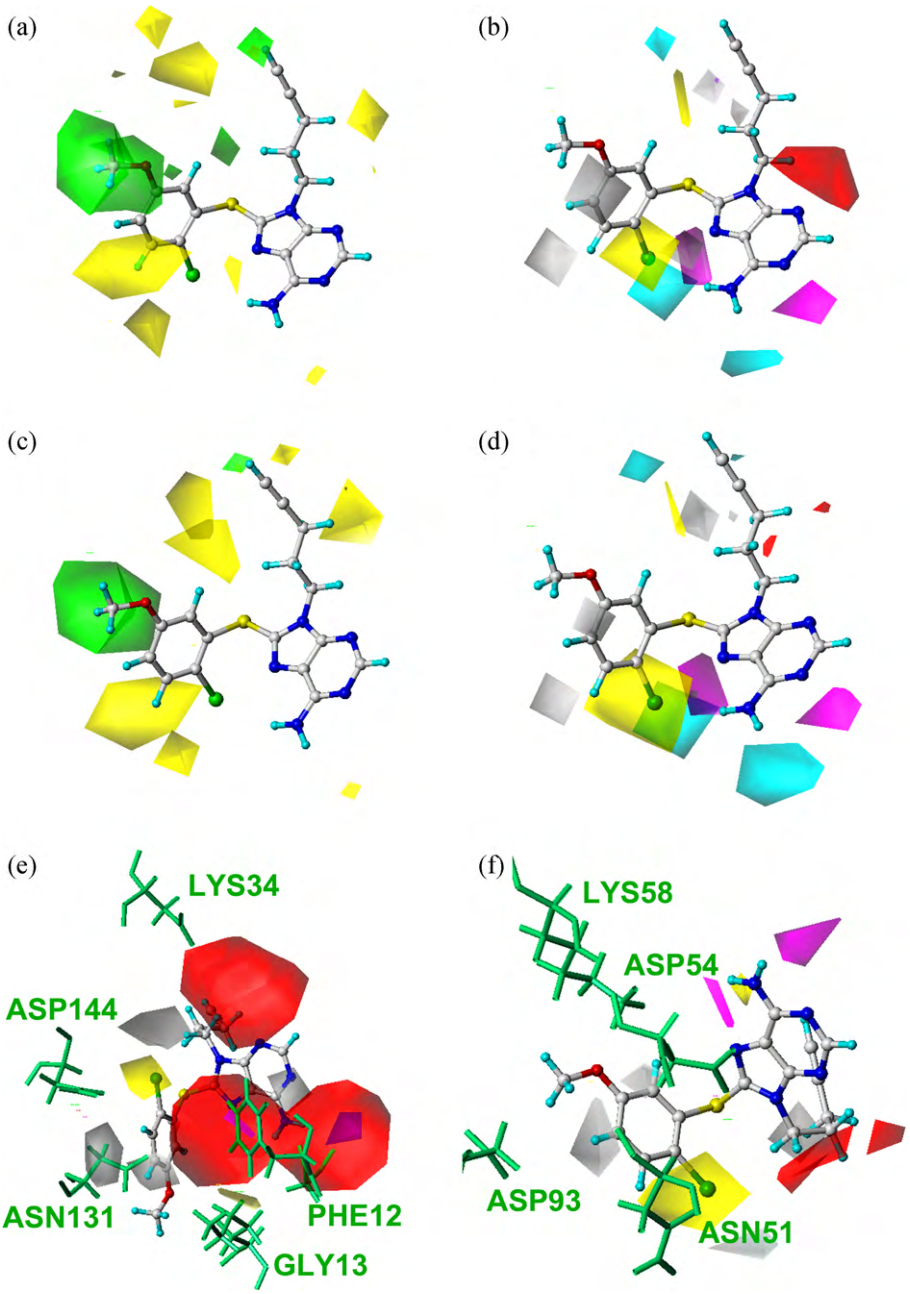

Fig. 2. The compound 11p in (a) the steric CoMFA contour maps for HER2, (b) the steric CoMFA contour maps for HSP90, (c) the CoMSIA contour maps for HER2, (d) the CoMSIA contour maps for HSP90, (e) the binding site of HER2 and (f) the binding site of HSP90. The contour maps of CoMFA represented to steric favor (green), steric disfavor (yellow) in (a) and (b). The contour maps of CoMSIA represented to hydrophobic favor (yellow), hydrophobic disfavor (white), electronegative favor (red), hydrogen bond donor favor (cyan), hydrogen bond donor disfavor (purple), and hydrogen bond acceptor favor (magenta). (For interpretation of the references to color in this figure legend, the reader is referred to the web version of the article.)

3.3. *The results of Hypogen*

The hypotheses of HER2 and HSP90 generated by Hypogen algorithm are listed in Tables 8 and 9, respectively. This protocol considers properties, such as hydrogen bond acceptor, hydrogen bond donor, and hydrophobic region. The fixed cost describes an ideal hypothesis model that could fit the data set perfectly. Contrast to the fixed cost, the null cost represents the model generated from compounds with the lowest activities. The difference between the null cost and the fixed cost of a precise hypothesis should be 40–60. This range of differences corresponds to 75–90% correlation for calculated and experiment activity. In addition, a precise hypothesis should be close to the fixed cost and far from the null cost. Accordingly, the first hypothesis of HER2 and HSP90 were selected for investigation. The reliability of the hypotheses was further validated by cat-scramble method (results see Fig. 5), and indeed, the initial runs were far from other random data sets in Fig. 5a and b.

To identify the differences between the Hypogen maps of HER2 and HSP90, the pharmacophore comparison protocol was employed. The results are shown in Table 10. The Hypogen maps of the two first hypotheses are shown in Fig. 6a and b. Both hypotheses shared similar features: one hydrophobic feature, one hydrogen bond donor, and two hydrogen bond acceptor features. However, despite both receptors have common pharmacophore features, the relative displacement between each feature in each receptor is

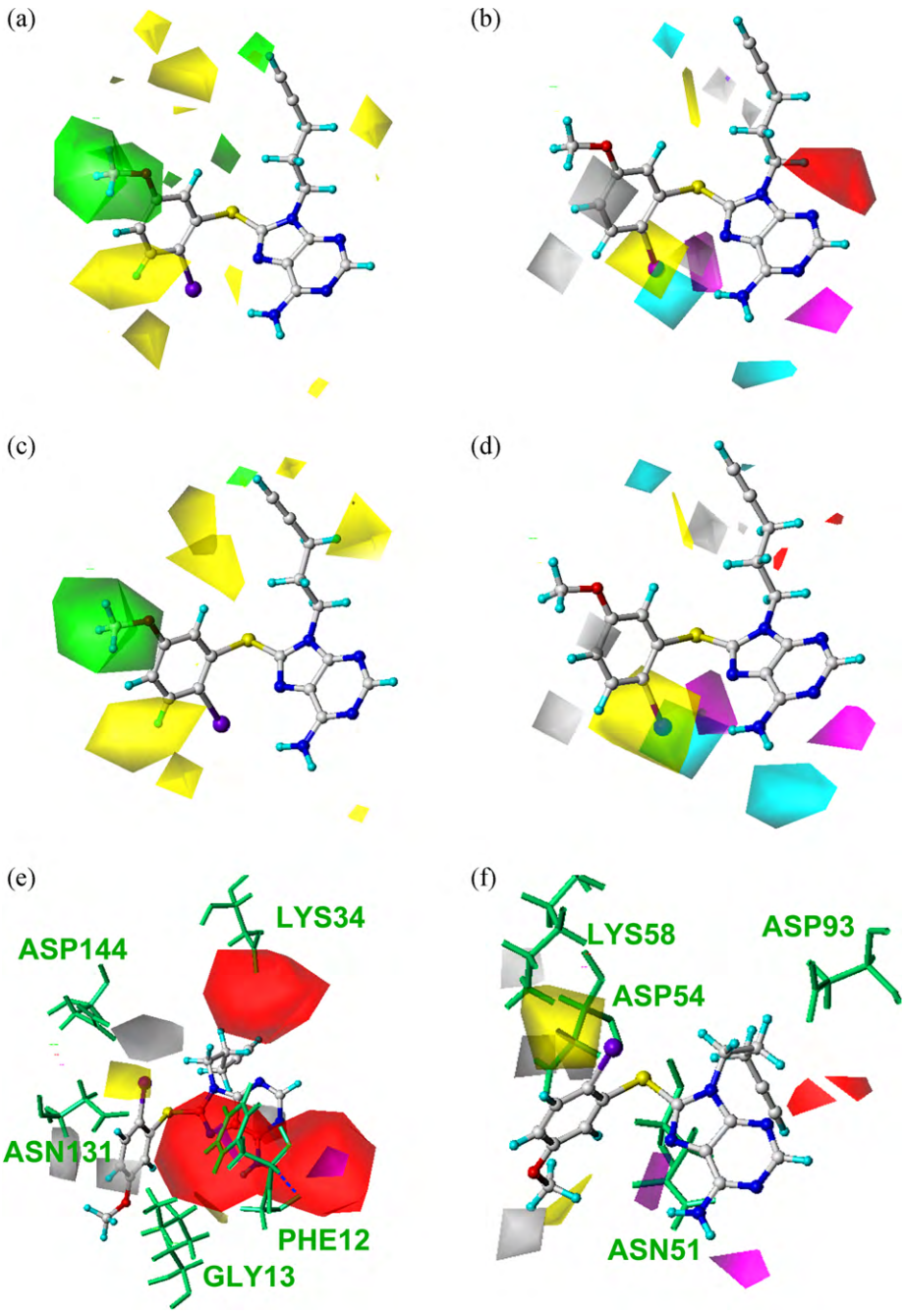

Fig. 3. The compound 11q in (a) the steric CoMFA contour maps for HER2, (b) the steric CoMFA contour maps for HSP90, (c) the CoMSIA contour maps for HER2, (d) the CoMSIA contour maps for HSP90, (e) the binding site of HER2 and (f) the binding site of HSP90. The contour maps of CoMFA represented to steric favor (green), steric disfavor (yellow) in (a) and (b). The contour maps of CoMSIA represented to hydrophobic favor (yellow), hydrophobic disfavor (white), electronegative favor (red), hydrogen bond donor favor (cyan), hydrogen bond donor disfavor (purple), and hydrogen bond acceptor favor (magenta). The hydrogen bonds were labeled by blue dot lines.

significantly different. A comparison of the hypotheses revealed large difference between the displacements of hydrophobic feature (value difference = 3.686) and a total RMSD difference of 2.002. These dissimilarities suggest that the pharmacophore maps cannot be superimposed and hence, cannot be combined to form a single hypothesis map.

To illustrate the hypothesis map of HER2 and HSP, compound 11v was used as an example. Compound 11v was able to fit into the two hypotheses, as shown in Fig. 4c and d. Notably, some conformation similarities were observed in Fig. 4c and d, especially at the purine-based main scaffold. However, the orientation of the remaining hydrogen bond acceptor features was distinct for each receptor. The C–S–C bond exhibited sharper angle in HER2 than in HSP90. Specifically, this bond angle appeared to be the determining factor for differential orientations. Therefore, in summary, dual-target inhibitors in this study should be able to have different orientations in HER2 and HSP90 in addition to properties discussed in the CoMFA and CoMSIA models.

3.4. The prediction analysis for CoMFA, CoMSIA, and Hypogen

To examine the predictivity of CoMFA, CoMSIA, and Hypogen models, we analyzed the correlation between experimental pIC_{50} and predicted pIC_{50}. For HER2, the R^2 values for CoMFA, CoMSIA,

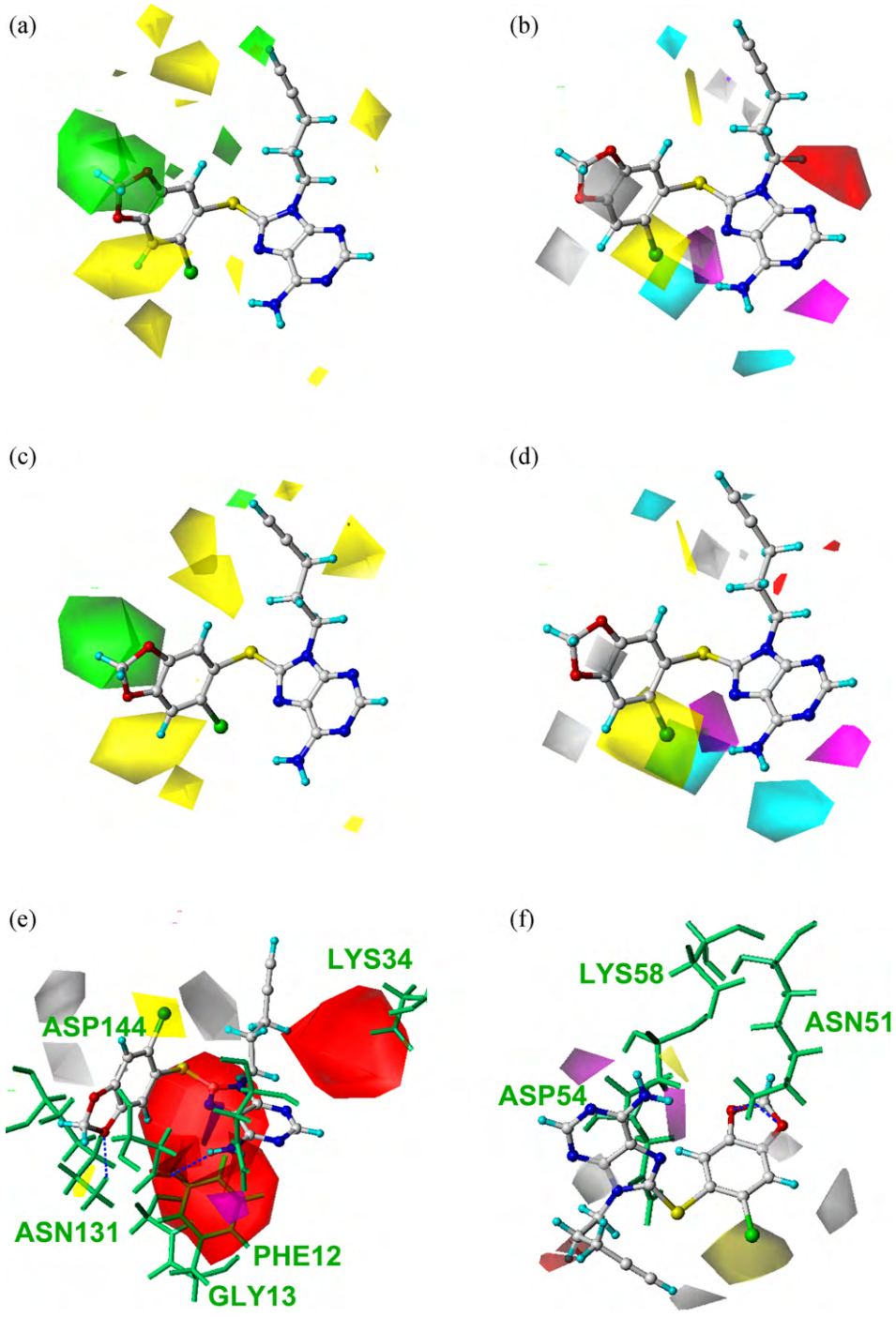

Fig. 4. The compound 11v in (a) the steric CoMFA contour maps for HER2, (b) the steric CoMFA contour maps for HSP90, (c) the CoMSIA contour maps for HER2, (d) the CoMSIA contour maps for HSP90, (e) the binding site of HER2 and (f) the binding site of HSP90. The contour maps of CoMFA represented to steric favor (green), steric disfavor (yellow) in (a) and (b). The contour maps of CoMSIA represented to hydrophobic favor (yellow), hydrophobic disfavor (white), electronegative favor (red), hydrogen bond donor favor (cyan), hydrogen bond donor disfavor (purple), and hydrogen bond acceptor favor (magenta). The hydrogen bonds were labeled by blue dot lines. (For interpretation of the references to color in this figure legend, the reader is referred to the web version of the article.)

and Hypogen were 0.884, 0.936, and 0.794, respectively. As for HSP90 the R^2 values for CoMFA, CoMSIA, and Hypogen were 0.922, 0.967, and 0.767. As shown in Fig. 7, the results suggest that the predictivity of Hypogen could be slightly lower than the CoMFA and CoMSIA models. Nevertheless, the R^2 value of Hypogen is still high enough to be significant. In addition, we also did multiple linear regression (Fig. 8), which yielded results similar to what shown in Fig. 7. This showed that the linear relationship observed in the training set is not a random event.

3.5. *The influence of flexibility on designing dual-targeted inhibitors*

The ligand binding poses from docking was analyzed. The bond angle of C–S–C bond in compound 11v was sharper in HER2 than in HSP90. Hydrogen bonds formations were also observed in both HER2 and HSP90. This observation would possibly need more experimental support but does not mean that a dual-target inhibitor cannot be obtained. Rather, this suggests that a

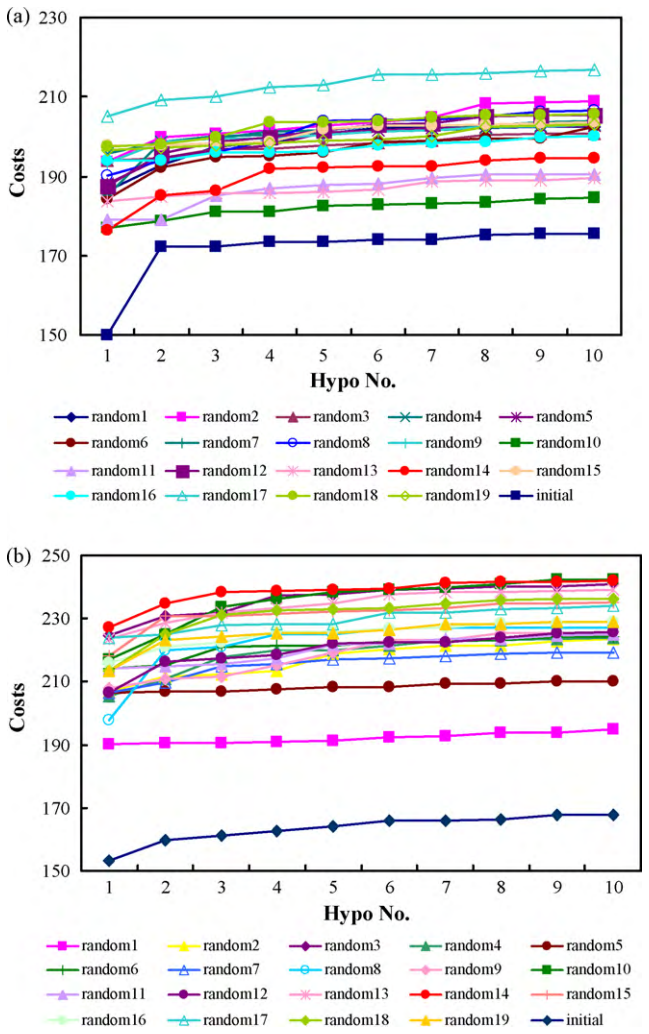

Fig. 5. The cat-scramble plot of HER2 (a) and HSP90 (b) in Hypogen. (For interpretation of the references to color in this figure legend, the reader is referred to the web version of the article.)

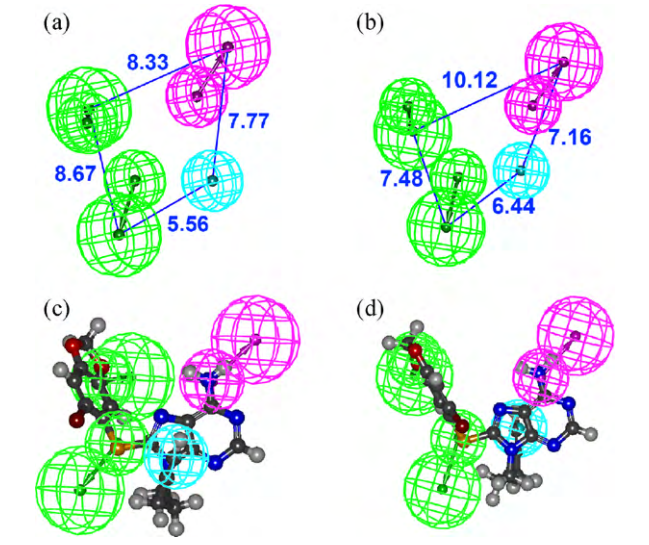

Fig. 6. The first hypothesis map of HER2 (a) and HSP90 (b). Illustrated queries hydrophobic (blue), hydrogen bond acceptor (green) and hydrogen bond donor (purple). The distances of features were labeled by blue lines. Compound 11v was fitted in the first hypothesis of Her2 (c) and the first hypothesis of HSP90 (d). (For interpretation of the references to color in this figure legend, the reader is referred to the web version of the article.)

Table 5
The CoMFA and CoMSIA test results of HSP90.

Name	CoMFA			CoMSIA	
	$pIC_{50\ exp}$	$pIC_{50\ pred}$	Residual	$pIC_{50\ pred}$	Residual
4	6.77	3.489	3.281	2.641	4.1291
11a	4.46	4.786	−0.3265	3.574	0.8861
11i	3.51	4.831	−1.3207	3.446	0.0641
28a	4.30	4.604	−0.3039	4.609	−0.3092
28b	4.22	3.568	0.6517	4.369	−0.1486
28c	4.30	4.476	−0.1757	4.487	−0.1866
28d	4.30	4.18	0.1205	4.421	−0.1213
28e	4.30	4.174	0.1256	4.308	−0.0076
28f	4.30	4.113	0.187	4.261	0.0385
30	5.44	3.752	1.6882	2.72	2.72
31	5.29	4.085	1.2053	3.015	2.2751
32	5.80	3.786	2.0138	2.776	3.0245

$pIC_{50\ exp}$: experimental pIC_{50}; $pIC_{50\ pred}$: predicted pIC_{50}.

HER2/HSP90 dual-target inhibitor could confer high receptor specificity and that flexibility must be present at the molecular hinge to keep the adaptability in both proteins. Unfortunately, such configuration requirement cannot be presented using the current QSAR model and thus, cannot be set as a criterion while screening the database.

In Llauger's studies [30,31], some of the compounds were noted for their anti-mitotic activities; these included compound 4, 11o, 11p, 11q, 12a, 30, 31, and 32 (Table 1 and Table S1). However, the anti-mitotic activity, as mentioned in Llauger's work, had no influence on binding affinity of the inhibitor to HER2 or HSP90. Our structural–activity relationship models had difficulties predicting the anti-mitotic activity, partly because the author did not quantify the activity. Therefore, the biological activity of compounds in the

Table 6
The CoMFA and CoMSIA prediction results of HER2.

Name	CoMFA			CoMSIA	
	$pIC_{50\ exp}$	$pIC_{50\ pred}$	Residual	$pIC_{50\ pred}$	Residual
11l	3.45	3.531	−0.0813	4.434	−0.9844
11m	3.83	3.702	0.1275	3.561	0.269
11n	4.58	4.024	0.5562	4.056	0.5241
11o	5.49	5.347	0.1434	5.346	0.1436
11p	5.84	5.798	0.0424	6.033	−0.1931
11q	6.09	5.913	0.1768	5.993	0.0966
11r	4.44	5.298	−0.8577	4.607	−0.1675
11s	4.22	4.318	−0.0976	4.321	−0.1008
11t	4	4.235	−0.2354	4.239	−0.2392
11u	4.24	3.987	0.2534	4.07	0.1702
11v	6.52	5.744	0.7764	6.029	0.4906
11w1	4.65	4.53	0.12	4.585	0.0646
11w2	4.05	3.977	0.0735	4.203	−0.1531
11w3	4.19	4.155	0.0355	4.246	−0.056
12a	5.46	5.544	−0.0844	5.475	−0.0153
12b	5.04	5.035	0.0047	4.776	0.2635
12c	5.3	5.623	−0.3227	5.436	−0.1356
12d	4.64	4.677	−0.0373	4.344	0.2956
12e	5.68	5.736	−0.0561	5.688	−0.0076
13	4	4.303	−0.3035	4.189	−0.1886
20a	4.68	4.705	−0.0246	4.544	0.1357
B9	4	3.851	0.149	3.785	0.2146
B10	3.44	3.759	−0.3188	3.621	−0.181
B11	4.3	4.015	0.285	4.349	−0.0495
B12	3.69	3.667	0.0233	3.732	−0.0423
B21	4.05	4.144	−0.0936	3.994	0.0562
B22	3.68	4.017	−0.3373	3.712	−0.0321
B23	3.52	3.887	−0.3673	3.493	0.0269
B25	4.1	3.575	0.5253	4.367	−0.2674
B31	1.3	1.335	−0.0346	1.113	0.1875
B32	1.3	1.441	−0.1407	1.2	0.1003
B33	1.52	1.419	0.1006	1.745	−0.2253

$pIC_{50\ exp}$: experimental pIC_{50}; $pIC_{50\ pred}$: predicted pIC_{50}.

Table 7
The CoMFA and CoMSIA prediction results of HSP90.

Name	CoMFA			CoMSIA	
	$pIC_{50\ exp}$	$pIC_{50\ pred}$	Residual	$pIC_{50\ pred}$	Residual
11l	4.43	4.451	−0.0212	5.37	−0.9396
11m	4.87	4.594	0.2765	4.633	0.2366
11n	5.68	5.083	0.5972	5.077	0.6034
11o	6.72	6.515	0.2052	6.645	0.075
11p	7.15	6.916	0.2342	7.324	−0.1738
11q	7.3	7.182	0.1182	7.281	0.0191
11r	5.43	6.401	−0.9714	5.638	−0.2084
11s	4.52	4.665	−0.1452	4.751	−0.231
11t	4.97	5.056	−0.0857	5.06	−0.0897
11u	5.07	5.146	−0.0762	4.955	0.1152
11v	7.52	6.949	0.5715	7.297	0.2227
11w1	5.82	5.645	0.1753	5.826	−0.0057
11w2	5.51	5.556	−0.0459	5.62	−0.1096
11w3	5.47	5.565	−0.0948	5.3	0.1705
12a	6.7	6.839	−0.1389	6.72	−0.0203
12b	6.74	6.674	0.0663	6.408	0.3316
12c	5.3	5.341	−0.0406	5.177	0.1225
12d	6.07	5.988	0.0817	5.997	0.0727
12e	5.68	5.631	0.0488	5.727	−0.0466
13	5.51	6.008	−0.4976	5.72	−0.21
20a	5.82	5.951	−0.1312	5.749	0.0714
B9	4.97	4.787	0.1831	4.658	0.3117
B10	4.3	4.682	−0.3818	4.54	−0.2397
B11	4.79	4.476	0.3141	4.651	0.1387
B12	4.41	4.296	0.1138	4.43	−0.0196
B21	4.65	4.714	−0.0641	4.59	0.0602
B22	4.25	4.589	−0.3393	4.381	−0.1311
B23	4.11	4.398	−0.2884	4.216	−0.1059
B25	4.3	3.945	0.3546	4.391	−0.0909
B31	1.82	1.892	−0.0719	1.619	0.2014
B32	1.82	1.977	−0.1565	1.84	−0.0202
B33	2.34	2.13	0.2104	2.45	−0.1105

$pIC_{50\ exp}$: experimental pIC_{50}; $pIC_{50\ pred}$: predicted pIC_{50}.

Table 8
The results of HER2 pharmacophore hypothesis generation.

Hypothesis	Total cost	Cost difference	Error cost	RMSD	*R* value	Features
1	150.11	59.13	126.37	1.082	0.909	AADH
2	172.30	36.94	154.32	1.708	0.735	AADH
3	172.34	36.90	153.65	1.696	0.740	AADH
4	173.35	35.89	154.41	1.710	0.736	AAD
5	173.55	35.69	155.62	1.731	0.726	AADH
6	173.91	35.33	155.95	1.738	0.724	AADH
7	174.10	35.14	155.63	1.727	0.729	ADR
8	175.29	33.95	156.70	1.751	0.719	AADH
9	175.47	33.77	156.89	1.755	0.718	ADHH
10	175.57	33.67	157.01	1.757	0.718	AAD

Null cost: 209.24. Fixed cost: 125.57. Configuration cost: 16.80. A, D, and H: hydrogen bond acceptor, hydrogen bond donor, and hydrophobic features, respectively.

Table 9
The results of HSP90 pharmacophore hypothesis generation.

Hypothesis	Total cost	Cost difference	Error cost	RMSD	*R* value	Features
1	153.20	85.82	132.26	1.240	0.902	AADH
2	159.96	79.06	132.57	1.248	0.907	AADH
3	161.40	77.62	140.65	1.436	0.866	AADH
4	162.73	76.29	143.62	1.499	0.852	AAAH
5	164.11	74.91	144.84	1.525	0.847	AADH
6	165.90	73.12	147.93	1.587	0.833	AADH
7	166.12	72.9	147.54	1.579	0.835	AADH
8	166.22	72.8	148.25	1.593	0.831	AADH
9	167.61	71.41	148.48	1.597	0.830	AADH
10	167.68	71.34	149.63	1.620	0.825	AADH

Null cost: 239.02. Fixed cost: 125.60. Configuration cost: 16.83. A, D, and H: hydrogen bond acceptor, hydrogen bond donor, and hydrophobic features, respectively.

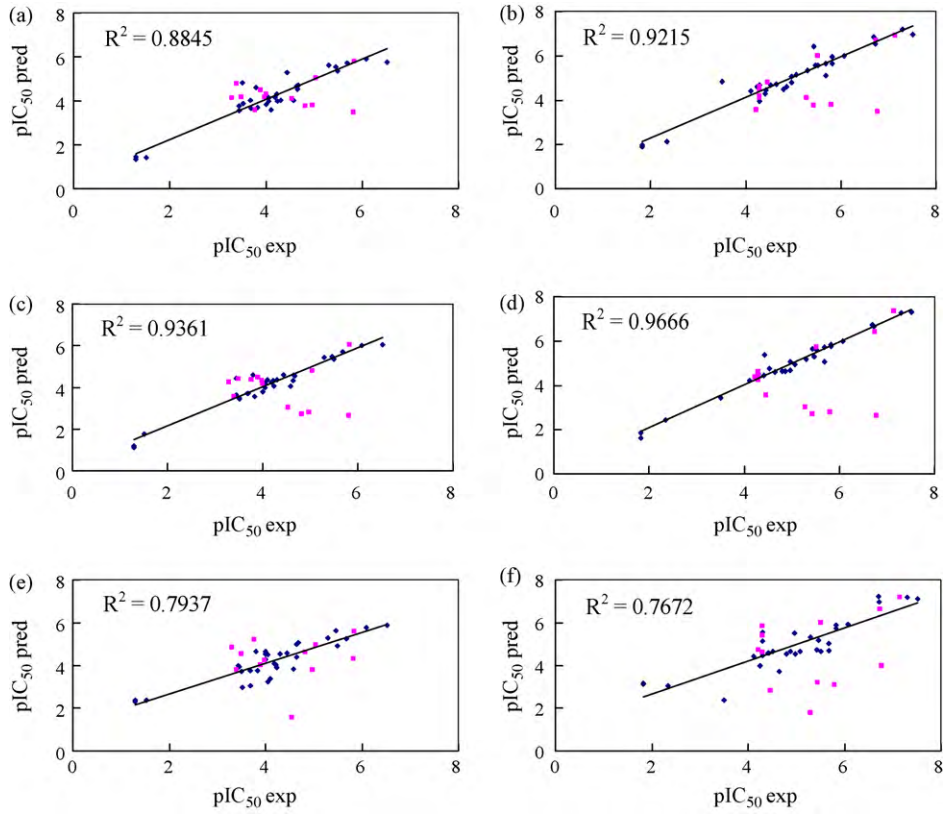

Fig. 7. The correlation in CoMFA model of HER2 (a), CoMFA model of HSP90 (b), CoMSIA model of HER2 (c), CoMSIA model of HSP90 (d), the first hypothesis of HER2 (e), and the first hypothesis of HSP90 (f). pIC_{50} exp is experimental pIC_{50} and pIC_{50} pred. is predicted pIC_{50}. The pink points are the test set in the plots. (For interpretation of the references to color in this figure legend, the reader is referred to the web version of the article.)

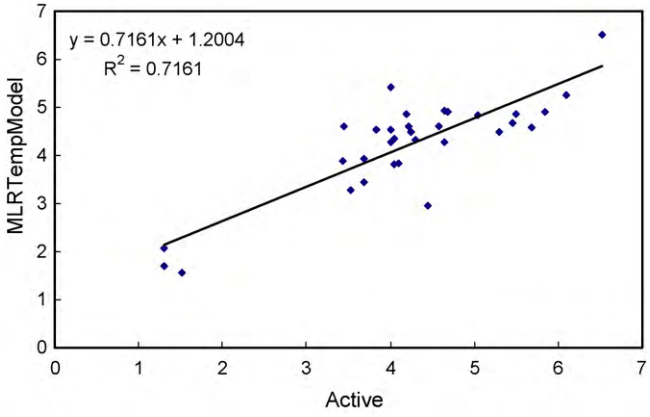

Fig. 8. The results of MLR model. [MLRTempModel] = 21.9795857802298 – 0.244475638786958 × [ALogP] + 0.840412176221228 × [Molecular_Solubility] + 1.045469385e−002 × [Molecular_Weight] + 1.65621679695339 × [Num_H_Acceptors] – 2.32213680964792 × [Num_H_Donors] – 2.22362207750852 × [Num_Rings] – 1.91095978538492 × [Num_RotatableBonds] – 18.1953717406255 × [Molecular_FractionalPolarSurfaceArea].

test set might be underestimated (Table 3 and Tables S4, S2 and S3). Unfortunately, we did not deduce a structure-relationship model form these anti-mitotic compounds. Therefore, the training set had excluded these small molecules, and we focused our research solely on investigating dual-target inhibitors. As for the excluded compounds, these will be our future investigation in addition to designing HER2/HSP90 dual-target inhibitors.

Table 10
The results of pharmacophore comparison for the first hypothesis of HER2 and HSP90.

Location	Displacement
Hydrophobic feature	3.686
HBD feature	1.149
HBA feature 1	1.382
HBA feature 2	2.353
Total RMSD	2.002

4. Conclusion

In this study, CoMFA model showed highly predictive r^2 values with 0.952 and 0.938 for HSP90 and HER2, respectively. In CoMSIA model, the r^2 values also showed as 0.967 and 0.961 for HSP90 and HER2, respectively. The contour maps indicated that the compounds had similar bulky favored area in HSP90 and HER2. Based on the CoMFA and CoMSIA results, the key criteria for designing a dual-target inhibitor for HSP90 and HER2 should consider the steric disfavor region in HSP90, and the electronegative favor and the hydrogen bond donor favor regions in HER2.

The Hypogen results for HER2 showed high cost difference and *r*-value as 59.13 and 0.909, respectively. Similarly, HSP90 also showed reliable cost difference and *r*-value, with 85.82 and 0.902, respectively. The first hypothesis maps of HER2 and HSP90 contained the same features: one hydrophobic feature, one hydrogen bond donor feature, and two hydrogen bond acceptor features. Although both receptors had similar hypotheses, the orientation of the pharmacophore features was distinctly different, especially for the hydrogen bond acceptor feature. Comparison of HER2 and HSP90 pharmacophores gave a RMSD of 2.002. These results sug-

gest that the effective compounds should have similar structural features but can adapt different poses in HER2 and HSP90 active sites.

Acknowledgements

The research was supported by grants from the National Science Council of China (NSC 98-2221-E-039-007), China Medical University (CMU98-CT-15, CMU97-276) and Asia University (CMU98-ASIA-09). This study is also supported in part by Taiwan Department of Health Clinical Trial and Research Center of Excellence (DOH99-TD-B-111-004) and Cancer Research Center of Excellence (DOH99-TD-C-111-005). We are grateful to the National Center of High-performance Computing for computer time and facilities.

Appendix A. Supplementary data

Supplementary data associated with this article can be found, in the online version, at doi:10.1016/j.jmgm.2010.04.002.

References

[1] F. Koga, K. Kihara, L. Neckers, Inhibition of cancer invasion and metastasis by targeting the molecular chaperone heat-shock protein 90, Anticancer Res. 29 (2009) 797–807.
[2] J. Buchner, HSP90 & Co.—a holding for folding, Trends Biochem. Sci. 24 (1999) 136–141.
[3] L. Whitesell, S.L. Lindquist, HSP90 and the chaperoning of cancer, Nat. Rev. Cancer 5 (2005) 761–772.
[4] C.Y.C. Chen, A novel perspective on designing the inhibitor of HER2 receptor, J. Chin. Inst. Chem. Eng. (2008) 291–299.
[5] Q. Ding, L. Huo, J.Y. Yang, W. Xia, Y. Wei, Y. Liao, C.J. Chang, Y. Yang, C.C. Lai, D.F. Lee, C.J. Yen, Y.J. Rita Chen, J.M. Hsu, H.P. Kuo, C.Y. Lin, F.J. Tsai, L.Y. Li, C.H. Tsai, M.C. Hung, Down-regulation of myeloid cell leukemia-1 through inhibiting Erk/Pin 1 pathway by sorafenib facilitates chemosensitization in breast cancer, Cancer Res. 68 (2008) 6109–6117.
[6] L. Neckers, HSP90 inhibitors as novel cancer chemotherapeutic agents, Trends Mol. Med. 8 (2002) 55–61.
[7] S.D. Satyanarayanajois, S. Ronald, Targeting HER2 Protein for breast cancer: exploring the chemical space of peptidomimetics for her2 binding using docking method, J. Biomol. Struct. Dynam. (2009) 870–1870.
[8] L. Neckers, K. Neckers, Heat-shock protein 90 inhibitors as novel cancer chemotherapeutic agents, Expert Opin. Emerg. Drugs 7 (2002) 277–288.
[9] J.C. Sheu, C.H. Hua, L. Wan, Y.J. Lin, H.C. Tseng, N. Jinawath, M.H. Tsai, N.W. Chang, C.F. Lin, C.C. Lin, L.J. Hsieh, T.L. Wang, I.M. Shih, F.J. Tsai, Functional genomic analysis identified EGFR activation as the most common genetic event in oral squamous cell carcinoma, Cancer Res. 69 (2009) 2568–2576.
[10] Y.J. Lin, Y.C. Hou, C.H. Lin, Y.A. Hsu, J.C. Sheu, C.H. Lai, B.H. Chen, P.D. Lee, L. Wan, F.J. Tsai, Puerariae radix isoflavones and their metabolites inhibit growth and induce apoptosis in breast cancer cells, Biochem. Biophys. Res. Commun. 378 (2009) 683–688.
[11] M. Awale, C.G. Mohan, 3D-QSAR CoMFA analysis of C5 substituted pyrrolotriazines as HER2 (ErbB2) inhibitors, J. Mol. Graph. Model. 26 (2008) 1169–1178.
[12] S. Benvenuti, P.M. Comoglio, The MET receptor tyrosine kinase in invasion and metastasis, J. Cell Physiol. 213 (2007) 316–325.
[13] A. De Luca, A. Carotenuto, A. Rachiglio, M. Gallo, M.R. Maiello, D. Aldinucci, A. Pinto, N. Normanno, The role of the EGFR signaling in tumor microenvironment, J. Cell Physiol. 214 (2008) 559–567.
[14] N. Normanno, A. De Luca, C. Bianco, L. Strizzi, M. Mancino, M.R. Maiello, A. Carotenuto, G. De Feo, F. Caponigro, D.S. Salomon, Epidermal growth factor receptor (EGFR) signaling in cancer, Gene 366 (2006) 2–16.
[15] C.Y.C. Chen, Discovery of novel inhibitors for c-Met by virtual screening and pharmacophore analysis, J. Chin. Inst. Chem. Eng. (2008) 617–624.
[16] C.Y.C. Chen, Computational screening and design of traditional Chinese medicine (TCM) to block phosphodiesterase-5, J. Mol. Graph. Model. (2009) 261–269.
[17] C.Y. Chen, Y.H. Chang, B.D. Tian, H.J. Huang, F.J. Tsai, C.H. Tsai, C.Y.C. Chen, Discovery of potent inhibitors for phosphodiesterase 5 by virtual screening and pharmacophore analysis, Acta Pharmacol. Sinica (2009) 1186–1194.
[18] C.Y.C. Chen, Weighted equation and rules—a novel concept for evaluating protein–ligand interaction, J. Biomol. Struct. Dynam. (2009) 271–282.
[19] C.Y. Chen, Y.H. Chang, B.D. Tian, H.J. Huang, F.J. Tsai, C.H. Tsai, C.Y.C. Chen, Ligand-based dual target drug design for H1N1: swine flu-A preliminary first study, J. Biomol. Struct. Dynam. (2009) 171–178.
[20] H.R. Bairagya, B.P. Mukhopadhyay, K. Sekar, An insight to the dynamics of conserved water molecular triad in IMPDH II (human): recognition of cofactor and substrate to catalytic Arg 322, J. Biomol. Struct. Dynam. (2009) 149–158.
[21] M.L. Bolognesi, A. Cavalli, L. Valgimigli, M. Bartolini, M. Rosini, V. Andrisano, M. Recanatini, C. Melchiorre, Multi-target-directed drug design strategy: from a dual binding site acetylcholinesterase inhibitor to a trifunctional compound against Alzheimer's disease, J. Med. Chem. 50 (2007) 6446–6449.
[22] M.J. de Jonge, J. Verweij, Multiple targeted tyrosine kinase inhibition in the clinic: all for one or one for all? Eur. J. Cancer 42 (2006) 1351–1356.
[23] N.S. Sapre, S. Gupta, N. Pancholi, N. Sapre, Data mining using template-based molecular docking on tetrahydroimidazo-[4,5,1-jk][1,4]-benzodiazepinone (TIBO) derivatives as HIV-1RT inhibitors, J. Mol. Model. 14 (2008) 1009–1021.
[24] J.C. Wojdel, First principles calculations on the influence of water-filled cavities on the electronic structure of Prussian Blue, J. Mol. Model. 15 (2005) 567–572.
[25] M.S. Gee, R. Upadhyay, H. Bergquist, R. Weissleder, L. Josephson, U. Mahmood, Multiparameter noninvasive assessment of treatment susceptibility, drug target inhibition and tumor response guides cancer treatment, Int. J. Cancer 121 (2007) 2492–2500.
[26] A. Petrelli, S. Giordano, From single- to multi-target drugs in cancer therapy: when aspecificity becomes an advantage, Curr. Med. Chem. 15 (2008) 422–432.
[27] C.Y.C. Chen, Bioinformatics, chemoinformatics, and pharmainformatics analysis of HER2/HSP90 dual-targeted inhibitors, J. Taiwan Inst. Chem. Eng. (2010) 143–149.
[28] A.J. Ryan, S.R. Wedge, ZD6474–a novel inhibitor of VEGFR and EGFR tyrosine kinase activity, Br. J. Cancer 92 (Suppl. 1) (2005) S6–13.
[29] S.N. Holden, S.G. Eckhardt, R. Basser, R. de Boer, D. Rischin, M. Green, M.A. Rosenthal, C. Wheeler, A. Barge, H.I. Hurwitz, Clinical evaluation of ZD6474, an orally active inhibitor of VEGF and EGF receptor signaling, in patients with solid, malignant tumors, Ann. Oncol. 16 (2005) 1391–1397.
[30] L. Llauger, H. He, J. Kim, J. Aguirre, N. Rosen, U. Peters, P. Davies, G. Chiosis, Evaluation of 8-arylsulfanyl, 8-arylsulfoxyl, and 8-arylsulfonyl adenine derivatives as inhibitors of the heat shock protein 90, J. Med. Chem. 48 (2005) 2892–2905.
[31] H. He, D. Zatorska, J. Kim, J. Aguirre, L. Llauger, Y. She, N. Wu, R.M. Immormino, D.T. Gewirth, G. Chiosis, Identification of potent water soluble purine-scaffold inhibitors of the heat shock protein 90, J. Med. Chem. 49 (2006) 381–390.
[32] J.C. Cole, C.W. Murray, J. Willem, M. Nissink, R.D. Taylor, R. Taylor, Comparing protein–ligand docking programs is difficult, Proteins 60 (2005) 325–332.
[33] Z. Wang, B. Ling, R. Zhang, Y. Suo, Y. Liu, Z. Yu, C. Liu, Docking and molecular dynamics studies toward the binding of new natural phenolic marine inhibitors and aldose reductase, J. Mol. Graph. Model. (2009) 162–169.